Robust Stability Analysis of a Multi-Input DC/DC Converter with Coupled Inductor for Renewable Energy Applications Based on Kharitonov's Theorem

Vahid Parvin Darabad and Reza Tamaskani

Abstract: **Previous studies have introduced a multi-input DC/DC converter with a coupled inductor to overcome the low output voltage of renewable energy sources (RESs), such as photovoltaic arrays (PVAs) and fuel cells. This converter provides a wide output-voltage range and effective power management at relatively low duty ratios. However, because its dynamics vary owing to uncertainties in component values, input voltages, and output load, its stability must be evaluated over a range of operating conditions. In this study, an uncertainty model is employed to describe the small-signal dynamics of the converter and to assess its robust stability. Kharitonov's theorem is then applied to establish a sufficient robust stability condition. To support this stability assessment, a Monte Carlo analysis is used to determine the extreme values of the characteristic polynomial coefficients under simultaneous component and load variations. The results show that all four Kharitonov polynomials satisfy the Routh stability criterion, demonstrating that the converter remains stable over the considered uncertainty range. This approach therefore provides a practical and effective framework for robust stability assessment of multi-input power converters intended for renewable-energy applications.**

Keywords: **Renewable energy source, multi-input converter, coupled inductor, robust stability, Kharitonov's theorem.**

I Introduction

The continuous growth in energy demand, increasing air pollution, and depletion of fossil-fuel resources have drawn considerable research attention to renewable energy sources (RESs), including solar and wind energy. To facilitate the coordinated utilization of multiple renewable sources, multi-port converters (MPCs) have received significant attention. In these converters, several input sources can independently or simultaneously supply a common output via a single integrated topology. One of the key objectives in DC/DC converter design is accurate output-voltage regulation with guaranteed stability under practical operating conditions [1], [2]. These conditions include uncertainties in the resistance, inductance, and capacitance values of the converter topology. Phenomena such as duty-cycle instability, undesirable voltage and current behavior, unwanted harmonics, and excessive ripple can adversely affect both the converter and the equipment connected to it. Consequently, stability analysis is essential for overall system performance, and newly proposed converter topologies require systematic stability assessment. An optimized converter design must therefore account not only for nominal operating performance but also for the robustness of its dynamic response against parameter variations.

Manuscript received 23 August 2026; revised 12 September 2026; accepted 20 September 2026.

V. Parvin Darabad is with the department of electrical engineering, faculty of engineering, Golestan University, Gorgan 15759-49138, Iran (e-mail: v.parvin@gu.ac.ir).

R. Tamaskani is with the department of electrical engineering, faculty of engineering, Golestan University, Gorgan 15759-49138, Iran (e-mail: reza_tamaskani@yahoo.com).

Corresponding author: V. Parvin Darabad.

A Literature

Early studies on the stability of switched-mode power converters employed averaged models [3], [4]. In these models, the periodic switching operation is neglected, and the resulting nonlinear model is linearized around an operating point. Over the past three decades, substantial effort has been devoted to developing design-oriented averaged models for switched converters, and many model variants have been reported in the literature. Although averaged models can accurately represent low-frequency or slow-scale converter dynamics, they cannot predict all nonlinear phenomena observed in switching systems because they neglect the switching action itself and the associated ripple in the state variables.

Since the pioneering work of Middlebrook and Ćuk [5] in the 1970s, several approaches have been developed to incorporate switching-related effects that conventional averaging cannot predict. In particular, improved averaging models [6], [7] have been proposed to predict the stable operating region. The approach in [8] incorporates a zero-order transfer function to account for the sampling effect of the modulator, whereas the method in [9] presents a general modeling procedure based on the Krylov–Bogoliubov–Mitropolsky ripple-estimation technique. Averaging-based modeling methods have been widely used to represent the switching dynamics of power converters. Applications of averaged modeling approaches for simulation using dedicated software packages such as RSPICE, SABER,

and MATLAB have also been widely reported [10], [11], [12]. As early as 1976, it was shown that state-space averaging has limited applicability for predicting stability when feedback signals contain high-frequency components at the switching frequency, as in peak-current and state-feedback control [13]–[15]. Therefore, more comprehensive approaches are required to account for the uncertainty and switching behavior of practical converters. Among the powerful analytical tools available for stability analysis, Kharitonov's theorem has attracted considerable attention because of its ability to evaluate the robust stability of interval polynomials [16]. Chang employed Kharitonov's theorem together with the LTR/LQG technique to design a controller for a state-voltage-controlled buck converter [17]. In [18], the robust controller design with fixed-structure for DC–DC converter was proposed using the Kharitonov approach. Meena and Singh applied Kharitonov's theorem to reduced-order modeling of a Ćuk converter, reducing the fourth-order model to first-, second-, and third-order models [19]. Kumar and Veerachary developed an analytical method for designing a robust non-fragile controller for load-voltage regulation of a high-gain boost converter that exhibits non-minimum-phase behavior due to a right-half-plane zero. Their method was based on the stability boundary locus and Kharitonov's theorem, providing a robust operating region with guaranteed gain and phase margins. Experimental results confirmed the effectiveness of the robust controller despite the performance limitations imposed by the right-half-plane zero [20].

B Contribution

An important consideration in the design of new converters is the operating mode. During the design stage, it is necessary to determine whether the converter operates in continuous conduction mode (CCM) or discontinuous conduction mode (DCM). An unintended transition between operating modes may disrupt the input–output relationship and lead to unstable behavior. Accordingly, the converter introduced in the authors' previous work is investigated in this paper from the perspective of robust stability by means of Kharitonov's criterion. The objective is to obtain an optimized stability assessment framework capable of accounting for simultaneous uncertainties in passive components, source voltages, and the output load. A recent approach to renewable energy integration is the use of multiple sources as inputs to converters. This approach offers several benefits. In particular, the series-switch configuration distributes the input voltage among multiple low-voltage, low-$R_{DS(on)}$ MOSFETs, significantly reducing per-device voltage stress and switching losses compared with a single high-voltage switch, while allowing different sources, such as solar PV panels and fuel cells, to supply the load simultaneously. Furthermore, this modular structure inherently provides fault tolerance and input-current sharing, which are highly desirable in distributed generation systems. The main contributions of this paper are summarized as follows:

1. Proposing a high-gain multi-input DC/DC converter topology based on coupled and switched inductors.
2. Deriving the complete small-signal state-space dynamic model of the multi-input converter in CCM.
3. Formulating the characteristic equation with interval coefficients that account for physical uncertainties.
4. Applying Kharitonov's theorem and the Routh–Hurwitz criterion to prove robust stability and determine the optimal stable parameter boundaries.
5. Verifying the theoretical stability margins through MATLAB/Simulink simulations under various severe operating conditions.

C Organization

Section II presents derives the averaged and small-signal state-space models in CCM,. Section III formulates the robust stability problem as an interval-polynomial problem, applies Kharitonov's theorem to to derive sufficient stability conditions. Section IV reports the simulation results. Finally, Section V concludes the main findings.

II Novel Multi-Input DC/DC Converter Based on SEPIC Structure

Figure 1 illustrates the converter proposed in the authors' previous work [21], [22]. The converter has a distinctive feature: its output can be supplied simultaneously by all N modules or by any individual input. Consequently, failure or removal of one input module does not disturb the output voltage. Figure 2 presents the internal structure of each module input.

A Modes of operation and state-Space equations

Defining the input vector $u^T = \begin{bmatrix} v_1 & v_2 \end{bmatrix}$ and the state vector $X^T = \begin{bmatrix} i_{L_1} & i_{L_2} & v_{C_1} & v_{C_2} \end{bmatrix}$, the state-space equations of the proposed converter, derived from its four operating modes, are presented as follows:

$$\dot{X} = A_i X + B_i u, \quad i = 1, \ldots, 4 \tag{1}$$

where

$$A_1 = \begin{bmatrix} 0 & 0 & 0 & 0 \\ 0 & 0 & \frac{1}{L_2} & 0 \\ 0 & -\frac{1}{C_1} & 0 & 0 \\ 0 & 0 & 0 & -\frac{1}{R_o C_2} \end{bmatrix}, \; B_1 = \begin{bmatrix} \frac{1}{L_1} & 0 \\ 0 & 0 \\ 0 & 0 \\ 0 & 0 \end{bmatrix}$$

$$A_2 = \begin{bmatrix} 0 & 0 & 0 & 0 \\ 0 & 0 & \frac{1}{L_2} & 0 \\ 0 & -\frac{1}{C_1} & 0 & 0 \\ 0 & 0 & 0 & -\frac{1}{R_o C_2} \end{bmatrix}, \; B_2 = \begin{bmatrix} 0 & \frac{1}{L_1} \\ 0 & 0 \\ 0 & 0 \\ 0 & 0 \end{bmatrix}$$

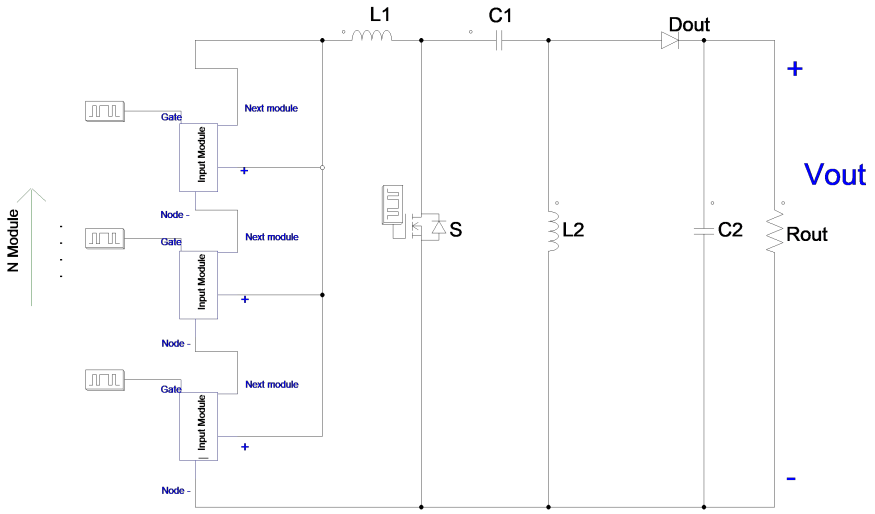


Fig. 1. Proposed converter topology.

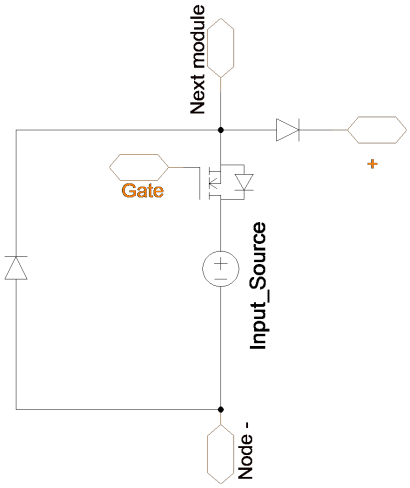


Fig. 2. Internal structure of a module input.

$$A_3 = \begin{bmatrix} 0 & 0 & 0 & 0 \\ 0 & 0 & \frac{1}{L_2} & 0 \\ 0 & -\frac{1}{C_1} & 0 & 0 \\ 0 & 0 & 0 & -\frac{1}{R_o C_2} \end{bmatrix}, \; B_3 = \begin{bmatrix} \frac{1}{L_1} & \frac{1}{L_2} \\ 0 & 0 \\ 0 & 0 \\ 0 & 0 \end{bmatrix}$$

$$A_4 = \begin{bmatrix} 0 & 0 & -\frac{1}{L_1} & -\frac{1}{L_1} \\ 0 & 0 & 0 & -\frac{1}{L_2} \\ \frac{1}{C_1} & 0 & 0 & 0 \\ \frac{1}{C_2} & \frac{1}{C_2} & 0 & -\frac{1}{R_o C_2} \end{bmatrix}, \; B_4 = \begin{bmatrix} 0 & 0 \\ 0 & 0 \\ 0 & 0 \\ 0 & 0 \end{bmatrix}$$

Applying the state-space averaging technique to the aforementioned equations yields the averaged state-space matrices as

$$\bar{A} = \begin{bmatrix} \bar{A}_{11} & \bar{A}_{12} \\ \bar{A}_{21} & \bar{A}_{22} \end{bmatrix}, \quad \bar{B} = \begin{bmatrix} \bar{B}_{11} \\ \bar{B}_{21} \end{bmatrix} \tag{2}$$

where

$$\bar{A}_{11} = \begin{bmatrix} 0 & 0 \\ 0 & 0 \end{bmatrix}$$

$$\bar{A}_{12} = \begin{bmatrix} -\frac{1-d_1-d_2-d_3}{L_1} & -\frac{1-d_1-d_2-d_3}{L_1} \\ \frac{d_1+d_2+d_3}{L_2} & -\frac{1-d_1-d_2-d_3}{L_2} \end{bmatrix}$$

$$\bar{A}_{21} = \begin{bmatrix} \frac{1-d_1-d_2-d_3}{C_1} & -\frac{d_1+d_2+d_3}{C_1} \\ \frac{1-d_1-d_2-d_3}{C_2} & \frac{1-d_1-d_2-d_3}{C_2} \end{bmatrix}$$

$$\bar{A}_{22} = \begin{bmatrix} 0 & 0 \\ 0 & -\frac{1}{R_o C_2} \end{bmatrix}$$

$$\bar{B}_{11} = \begin{bmatrix} \frac{d_1+d_3}{L_1} & \frac{d_2+d_3}{L_1} \\ 0 & 0 \end{bmatrix}$$

$$\bar{B}_{21} = \begin{bmatrix} 0 & 0 \\ 0 & 0 \end{bmatrix}$$

Furthermore, to elucidate the possible operating conditions of the proposed topology, Fig. 3 depicts practical operating scenarios for the converter (with $N = 2$). This figure demonstrates the possible combinations of

input sources and switching states while clarifying the operating mechanism. To derive the small-signal model, perturbations are applied to the state, input, and control variables. Each variable comprises a DC component and a perturbation component, expressed as follows:

$$\begin{aligned} i_{L_1} &= I_{L_1} + \hat{i}_{L_1}, & i_{L_2} &= I_{L_2} + \hat{i}_{L_2} \\ v_{C_1} &= V_{C_1} + \hat{v}_{C_1}, & v_{C_2} &= V_{C_2} + \hat{v}_{C_2} \\ v_1 &= V_1 + \hat{v}_1, & v_2 &= V_2 + \hat{v}_2 \\ d_1 &= D_1 + \hat{d}_1, & d_2 &= D_2 + \hat{d}_2 \\ d_3 &= D_3 + \hat{d}_3 \end{aligned} \tag{3}$$

where uppercase variables denote the DC components, while variables marked with a hat ($\hat{\cdot}$) represent the corresponding perturbation components. By linearizing the equations around the operating point and neglecting the higher-order perturbation terms, the DC components are eliminated, resulting in:

$$\begin{aligned} \frac{d\hat{i}_{L_1}}{dt} &= \frac{\hat{d}_1 + \hat{d}_2 + \hat{d}_3}{L_1}(V_{C_1} + V_{C_2}) \\ &\quad - \frac{1 - D_1 - D_2 - D_3}{L_1}(\hat{v}_{C_1} + \hat{v}_{C_2}) \\ &\quad + \frac{\hat{d}_1 + \hat{d}_3}{L_1}V_1 + \frac{\hat{d}_2 + \hat{d}_3}{L_1}V_2 \\ &\quad + \frac{D_1 + D_3}{L_1}\hat{v}_1 + \frac{D_2 + D_3}{L_1}\hat{v}_2 \end{aligned} \tag{4}$$

$$\begin{aligned} \frac{d\hat{i}_{L_2}}{dt} &= \frac{D_1 + D_2 + D_3}{L_2}\hat{v}_{C_1} - \frac{1 - D_1 - D_2 - D_3}{L_2}\hat{v}_{C_2} \\ &\quad + \frac{\hat{d}_1 + \hat{d}_2 + \hat{d}_3}{L_2}(V_{C_1} + V_{C_2}) \end{aligned} \tag{5}$$

$$\begin{aligned} \frac{d\hat{v}_{C_1}}{dt} &= \frac{1 - D_1 - D_2 - D_3}{C_1}\hat{i}_{L_1} - \frac{D_1 + D_2 + D_3}{C_1}\hat{i}_{L_2} \\ &\quad - \frac{\hat{d}_1 + \hat{d}_2 + \hat{d}_3}{C_1}(I_{L_1} + I_{L_2}) \end{aligned} \tag{6}$$

$$\begin{aligned} \frac{d\hat{v}_{C_2}}{dt} &= \frac{1 - D_1 - D_2 - D_3}{C_2}\hat{i}_{L_1} + \frac{1 - D_1 - D_2 - D_3}{C_2}\hat{i}_{L_2} \\ &\quad - \frac{1}{R_o C_2}\hat{v}_{C_2} \end{aligned} \tag{7}$$

Small-signal analysis of the converter yields the following state-space matrix equations for continuous-conduction operation:

$$\begin{bmatrix} \frac{d\hat{i}_{L_1}}{dt} \\ \frac{d\hat{i}_{L_2}}{dt} \\ \frac{d\hat{v}_{C_1}}{dt} \\ \frac{d\hat{v}_{C_2}}{dt} \end{bmatrix} = A \begin{bmatrix} \hat{i}_{L_1} \\ \hat{i}_{L_2} \\ \hat{v}_{C_1} \\ \hat{v}_{C_2} \end{bmatrix} + B \begin{bmatrix} \hat{d}_1 \\ \hat{d}_2 \\ \hat{d}_3 \end{bmatrix} + C \begin{bmatrix} \hat{v}_1 \\ \hat{v}_2 \end{bmatrix} \tag{8}$$

where A, B, and C are the state, control-input, and input-disturbance matrices, respectively. For a given converter operating point, the entries of these matrices depend on the duty ratios D_1, D_2, and D_3, the inductances L_1 and L_2, the capacitances C_1 and C_2, the load resistance R_o, the capacitor voltages V_{C_1} and V_{C_2}, the inductor currents I_{L_1} and I_{L_2}, and the input voltages V_1 and V_2.

The system matrices A, B, and C have the following structure:

$$\begin{aligned} A &= \begin{bmatrix} A_{11} & A_{12} \\ A_{21} & A_{22} \end{bmatrix} \\ B &= \begin{bmatrix} B_{11} & B_{12} \\ B_{21} & B_{22} \end{bmatrix} \\ C &= \begin{bmatrix} C_{11} & C_{12} \\ C_{21} & C_{22} \end{bmatrix} \end{aligned} \tag{9}$$

where

$$A_{11} = \begin{bmatrix} 0 & 0 \\ 0 & 0 \end{bmatrix},\ A_{22} = \begin{bmatrix} 0 & 0 \\ 0 & -\frac{1}{R_o C_2} \end{bmatrix}$$

$$A_{12} = \begin{bmatrix} -\frac{1 - D_1 - D_2 - D_3}{L_1} & -\frac{1 - D_1 - D_2 - D_3}{L_1} \\ \frac{D_1 + D_2 + D_3}{L_2} & -\frac{1 - D_1 - D_2 - D_3}{L_2} \end{bmatrix}$$

$$A_{21} = \begin{bmatrix} \frac{1 - D_1 - D_2 - D_3}{C_1} & -\frac{D_1 + D_2 + D_3}{C_1} \\ \frac{1 - D_1 - D_2 - D_3}{C_2} & \frac{1 - D_1 - D_2 - D_3}{C_2} \end{bmatrix}$$

$$B_{11} = \begin{bmatrix} \frac{V_{C_1} + V_{C_2} + V_1}{L_1} & \frac{V_{C_1} + V_{C_2} + V_2}{L_1} \\ \frac{V_{C_1} + V_{C_2}}{L_2} & \frac{V_{C_1} + V_{C_2}}{L_2} \end{bmatrix}$$

$$B_{12} = \begin{bmatrix} \frac{V_{C_1} + V_{C_2} + V_1 + V_2}{L_1} \\ \frac{V_{C_1} + V_{C_2}}{L_2} \end{bmatrix}$$

$$B_{21} = \begin{bmatrix} -\frac{I_{L_1} + I_{L_2}}{C_1} & -\frac{I_{L_1} + I_{L_2}}{C_1} \\ 0 & 0 \end{bmatrix}$$

$$B_{22} = \begin{bmatrix} -\frac{I_{L_1} + I_{L_2}}{C_1} \\ 0 \end{bmatrix}$$

$$C_{11} = \begin{bmatrix} \frac{D_1 + D_3}{L_1} \\ 0 \end{bmatrix},\ C_{12} = \begin{bmatrix} \frac{D_2 + D_3}{L_1} \\ 0 \end{bmatrix}$$

$$C_{21} = C_{22} = \begin{bmatrix} 0 \\ 0 \end{bmatrix}$$

The matrices B and C depend on the steady-state capacitor voltages, input voltages, and inductor currents. In particular, the matrix B contains terms proportional to $\frac{V_{C_1} + V_{C_2} + V_1}{L_1}$, $\frac{V_{C_1} + V_{C_2} + V_2}{L_1}$, $\frac{V_{C_1} + V_{C_2} + V_1 + V_2}{L_1}$, and $\frac{I_{L_1} + I_{L_2}}{C_1}$, whereas the matrix C includes duty-ratio-dependent terms such as $\frac{D_1 + D_3}{L_1}$ and $\frac{D_2 + D_3}{L_1}$.

The characteristic equation of the linearized converter

about its operating point is described by

$$\det(sI - A) = 0 \tag{10}$$

Since the converter parameters are uncertain, the coefficients of this characteristic equation are not constant; rather, they lie within prescribed intervals.

III Robust Stability Analysis via Kharitonov's Theorem

A Formulation of interval polynomials

Under real operating conditions, the converter components vary within known physical bounds:

$$\begin{aligned} L_j &\in \left[L_j^{\min}, L_j^{\max}\right], \quad C_j \in \left[C_j^{\min}, C_j^{\max}\right], \\ R_L &\in \left[R_L^{\min}, R_L^{\max}\right], \quad D \in \left[D^{\min}, D^{\max}\right] \end{aligned} \tag{11}$$

Consequently, the coefficients of the characteristic polynomial lie within closed intervals:

$$a_i \in \left[a_i^{\min}, a_i^{\max}\right] \tag{12}$$

The family of uncertain characteristic polynomials is defined as:

$$P(s) = \sum_{i=0}^{n} a_i s^i, \quad a_i \in \left[a_i^{\min}, a_i^{\max}\right] \tag{13}$$

B Kharitonov's stability theorem

According to Kharitonov's theorem, the entire interval family of polynomials $P(s)$ is Hurwitz stable, i.e., all its roots lie strictly in the open left half of the complex plane, if and only if the four extreme Kharitonov polynomials are Hurwitz stable:

$$\begin{aligned} K_1(s) &= a_0^{\min} + a_1^{\min} s + a_2^{\max} s^2 + a_3^{\max} s^3 + \cdots \\ K_2(s) &= a_0^{\max} + a_1^{\max} s + a_2^{\min} s^2 + a_3^{\min} s^3 + \cdots \\ K_3(s) &= a_0^{\max} + a_1^{\min} s + a_2^{\min} s^2 + a_3^{\max} s^3 + \cdots \\ K_4(s) &= a_0^{\min} + a_1^{\max} s + a_2^{\max} s^2 + a_3^{\min} s^3 + \cdots \end{aligned} \tag{14}$$

C Routh–Hurwitz stability criteria for $K_m(s)$

For a generic fourth-order polynomial $K(s) = c_4 s^4 + c_3 s^3 + c_2 s^2 + c_1 s + c_0$, the Routh array is constructed in Table 1. For Hurwitz stability, the necessary and sufficient conditions are:

1. $c_i > 0$, for all $i \in \{0, 1, 2, 3, 4\}$
2. $b_1 > 0 \Longrightarrow c_3 c_2 - c_4 c_1 > 0$
3. $c_1' > 0 \Longrightarrow (c_3 c_2 - c_4 c_1) c_1 - c_3^2 c_0 > 0$

Evaluating these conditions for each of the four Kharitonov polynomials ($K_1(s)$, $K_2(s)$, $K_3(s)$, $K_4(s)$) establishes the optimal bounds on passive component selection and duty-cycle control limits.

IV Simulation and Results

The converter parameters used in the simulation are listed in Table 2. A central challenge in applying Kharitonov's theorem to the proposed converter is that the exact minimum and maximum values of the characteristic-polynomial coefficients are not available in closed form. Since these coefficients depend on complex algebraic expressions involving the converter inductances and capacitances, their extrema cannot be readily obtained through direct analytical manipulation. Therefore, the approach adopted in this study relies on Monte Carlo analysis to estimate these bounds.

TABLE 1. The Routh--Hurwitz table for fourth-order polynomial.

s^4	c_4	c_2	c_0
s^3	c_3	c_1	0
s^2	$b_1 = \dfrac{c_3 c_2 - c_4 c_1}{c_3}$	c_0	0
s^1	$c_1' = \dfrac{b_1 c_1 - c_3 c_0}{b_1}$	0	0
s^0	c_0	0	0

TABLE 2. Converter parameters.

Parameter	Value
V_1	12 V
V_2	20 V
V_0	48 V
P_0	230 W
$\sum_{i=1}^{3} D_i$	0.5
f_s	10 kHz
L_1	20 mH
L_2	20 mH
C_1	10 µF
C_2	750 µF
R_1	10 Ω

TABLE 3. Minimum and maximum values of coefficients.

Coefficient	Minimum	Maximum
a_4	1	1
a_3	116.382	155.159
a_2	1.1552×10^6	1.3938×10^6
a_1	6.9321×10^8	9.9809×10^8
a_0	6.9884×10^{10}	9.7928×10^{10}

TABLE 4. The first column of the Routh arrays.

Routh-array entry	$K_1(s)$	$K_2(s)$	$K_3(s)$	$K_4(s)$
Row 1	1	1	1	1
Row 2	1.5436×10^2	1.1563×10^2	1.5436×10^2	1.1563×10^2
Row 3	9.3242×10^5	4.9976×10^5	7.0980×10^5	2.7714×10^5
Row 4	6.3032×10^7	8.5774×10^7	4.8611×10^7	6.1875×10^7
Row 5	7.0926×10^{10}	7.0926×10^{10}	9.6612×10^{10}	9.6612×10^{10}

To quantify the effect of component and load uncertainties on the characteristic polynomial, a Monte Carlo analysis was performed by considering simultaneous variations in the uncertain parameters C_1, C_2, L_1, L_2, and R_0. The capacitances and inductances were assumed to vary independently within ±5% of their nominal values, while the load resistance was allowed to vary within ±10%. For each Monte Carlo realization, all uncertain parameters were randomly sampled simultaneously within their specified uncertainty intervals, and the resulting parameter set was used to calculate the characteristic-polynomial coefficients b, c, d, and e from their corresponding analytical expressions. In this analysis, 100,000 independent realizations were generated to improve the reliability of the estimated coefficient bounds. The minimum and maximum

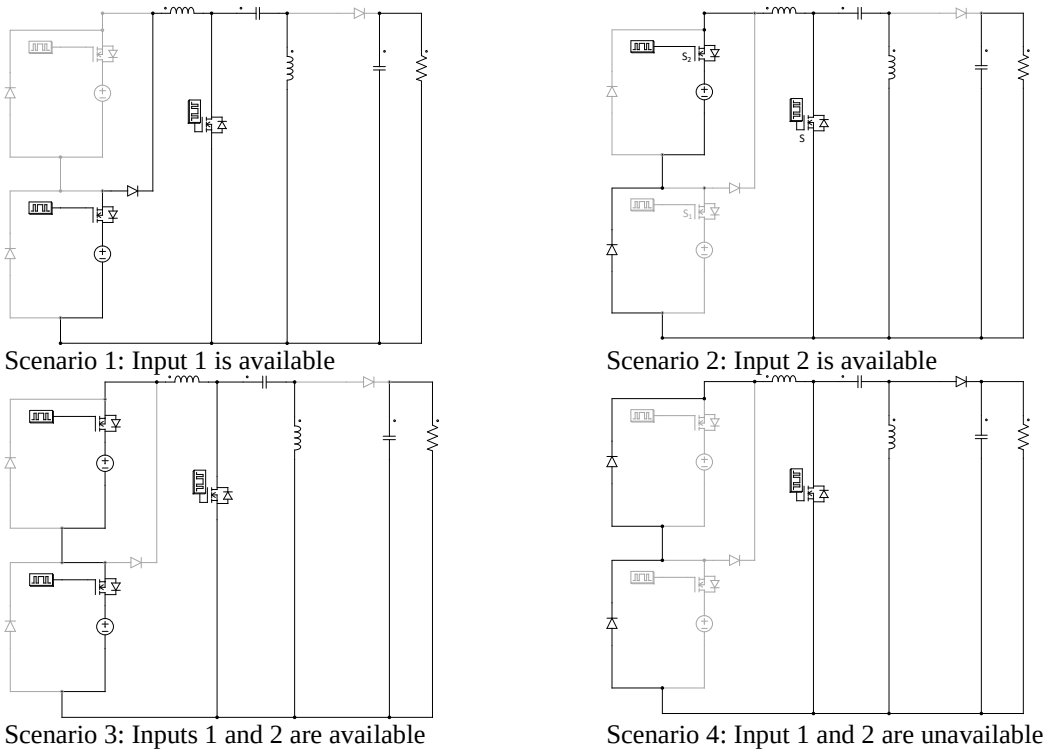


Fig. 3. Internal modes of operation.

values of each coefficient were then obtained by searching over all generated realizations, i.e., $b_{\min} = \min_k b^k$, $b_{\max} = \max_k b^k$, and similarly for c, d, and e, where $k = 1, \ldots, 100{,}000$. Importantly, the corresponding values of C_1, C_2, L_1, L_2, and R_0 associated with each minimum and maximum coefficient were also recorded. These extracted bounds were subsequently used to construct the interval polynomial family required for the Kharitonov robust-stability analysis. Table 3 lists the estimated minimum and maximum values of the characteristic-polynomial coefficients obtained through MATLAB-based Monte Carlo simulation. For each of the four Kharitonov polynomials, a Routh table was constructed, and the first-column entries of the resulting Routh arrays are reported in Table 4. As shown in Table 4, all entries in the first column are positive for each of the four Kharitonov polynomials; thus, the original characteristic polynomial remains stable over the considered uncertainty range. Hence, the proposed multi-input DC/DC converter satisfies the required robust stability condition under the simultaneous variations considered in the Monte Carlo study.

To further verify the robust stability results, MATLAB/Simulink simulations were performed for three representative parameter conditions: the nominal parameter set, the parameter combination associated with the lower-bound coefficients, and that associated with the upper-bound coefficients. The corresponding output-voltage responses are shown in Fig. 4. Although the boundary cases exhibit different transient behaviors and higher overshoot than the nominal case, all three responses converge to a bounded steady-state value without divergence. This behavior confirms stable operation of the converter under the selected parameter-bound conditions and is consistent with the robust stability results obtained using Kharitonov's theorem.

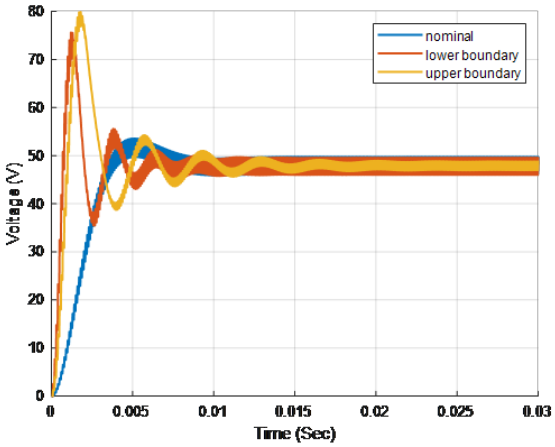


Fig. 4. Output-voltage responses under nominal, lower-bound, and upper-bound parameter conditions.

V Conclusions

Modeling methods for power-electronic converters provide a fundamental basis for the analysis and design of switching power stages. Numerous modeling approaches are available, and their suitability depends on the required accuracy and the operating-frequency range. This

study provides a practical framework for robust stability analysis of power-electronic converters in the presence of parameter uncertainties. The resulting methodology can help researchers and engineers develop optimized design procedures and select appropriate stability-analysis tools for different converter topologies. One advantage of the state-space averaging method is its straightforward implementation and its acceptable low-frequency accuracy in predicting converter behavior. Generalized averaging models can provide greater accuracy because switching ripple is explicitly taken into account; however, this improvement increases the number of state variables and, consequently, the complexity of the system model. In this paper, the robust stability of a complex multi-input DC/DC converter is investigated. Conventional μ-synthesis and H_∞-based approaches may lead to high-order controllers and significant computational complexity. In contrast, the proposed analysis is formulated using the four Kharitonov endpoint polynomials, providing a comparatively simple procedure for assessing robust stability without requiring a complicated controller synthesis framework, weighting functions, or high-order optimization procedures. The results demonstrate that Kharitonov's theorem is suitable for establishing the robust stability of the proposed DC/DC converter over the specified ranges of component and load uncertainties. The combination of interval-polynomial analysis and Monte Carlo estimation provides an effective and practical approach for robust stability verification and can be extended to other power-converter topologies and robust-control studies.

References

[1] Saadat, S.A., *et al.* Improved robust adaptive cascade control of buck converters using complex-order PSO algorithm: theory and experiments, *International Journal of Dynamics and Control*, vol. 13, no. 10, p. 357, 2025.

[2] Keighobadi, J., Saadat, S.A., Alfi, A., Current-sensorless robust optimal sequential learning control of buck converters: Theoretical framework and experimental validation, *Iranian Journal of Science and Technology, Transactions of Electrical Engineering*, vol. 50, pp. 2969–2986, 2026.

[3] Kassakian, J.G., Schlecht, M.F., Verghese, G.C., *Principles of Power Electronics*, New York: Springer, 1991.

[4] Azer, P., Emadi, A., Generalized state space average model for multi-phase interleaved buck, boost and buck-boost DC-DC converters: Transient, steady-state and switching dynamics, *IEEE Access*, vol. 8, pp. 77735-77745, 2020.

[5] Middlebrook, R.D., Ćuk, S., A general unified approach to modeling switching-converter power stages, in *Proc. Power Electronics Specialists Conference*, 1976, pp. 18–34.

[6] Caliskan, V.A., Verghese, G.C., Stanković, A.M., Multifrequency averaging of DC/DC converters, *IEEE Trans. Power Electron.*, vol. 14, no. 1, pp. 124-133, Jan. 1999.

[7] Alrajhi, H., A generalized state space average model for parallel DC-to-DC converters, *Computer Systems Science & Engineering*, vol. 41, no. 2, 2022.

[8] Ridley, R.B., A new, continuous-time model for current-mode control, *IEEE Transactions on Power Electronics*, vol. 6, no. 2, pp. 271-280, 1991.

[9] Sun, J., Characterization and performance comparison of ripple-based control for voltage regulator modules, *IEEE Trans. Power Electron.*, vol. 21, no. 2, pp. 346-353, 2006.

[10] Erickson, R.W., Maksimović, D., *Fundamentals of power electronics*, 2nd ed. New York: Springer, 2001.

[11] Peng, C., *et al.*, Design of a novel robust adaptive fractional-order model predictive controller for boost converter using grey wolf optimization algorithm, *Scientific Reports*, vol. 15, no. 1, p. 27670, 2025.

[12] Ghamari, S.M., Aziz, A., A universal hybrid model-free deep quantum–transfer learning controller enhanced by grey wolf optimization for DC–DC boost converters with hardware-in-the-loop validation, *IET Power Electronics*, vol. 19, no. 1, p. e70263, 2026.

[13] Yue, X., Wang, X., Blaabjerg, F., Review of small-signal modeling methods including frequency-coupling dynamics of power converters, *IEEE Transactions on Power Electronics*, vol. 34, no. 4, pp. 3313-3328, 2019.

[14] Guo, Y., *et al.*, Stability-improvement method of cascaded DC-DC converters with additional voltage-error mutual feedback control, *Chinese Journal of Electrical Engineering*, vol. 5, no. 2, pp. 63-71, 2019.

[15] Andresen, M., Kuprat, J., Raveendran, V., *et al.* Active thermal control for delaying maintenance of power electronics converters, *Chinese Journal of Electrical Engineering*, vol. 4, no. 3, pp. 13-20, 2018.

[16] Ebrahimi, M., Alaviyan Shahri, E.S., Alfi, A., A graphical method-based Kharitonov theorem for robust stability analysis of incommensurate fractional-order uncertain systems, *Computational and Applied Mathematics*, vol. 43, no. 2, p. 101, 2024.

[17] Chang, C., Robust control of DC-DC converters: the buck converter, In: *Proceedings of PESC'95-Power Electronics Specialist Conference*, vol. 2, pp. 1094-1097, IEEE, 1995.

[18] Sedehi, A.G., Alfi, A., Swarm-based robust fixed-structure controller design for buck converter using Kharitonov approach: design and experiment, *International Journal of Dynamics and Control*, vol. 10, no. 4, pp. 1251-1264, 2022.

[19] Meena, V.P., Singh, V.P., Kharitonov polynomial-based interval reduced order modelling of Ćuk converter, *International Journal of Modelling, Identification and Control*, vol. 41, no. 3, pp. 231-242, 2022.

[20] Cui, T., Ma, Q., Xu, P., Sufficient condition-based stability analysis of a power converter applied switching transient waveform modification using Kharitonov's theorem, *Electronics*, vol. 8, no. 2, p. 245, 2019.

[21] Parvin Darabad, V., A novel multi-input DC/DC converter with a coupled and switched inductor applicable to renewable energy sources, In: *Proceedings of the Second National Conference on New Business in Electrical and Computer Engineering*, Khorramabad, 2024.

[22] Parvin Darabad, V., Small-signal analysis of a novel multi-input DC/DC converter with a coupled and switched inductor applicable to renewable energy sources for stability studies, In: *Proceedings of the Second National Conference on New Business in Electrical and Computer Engineering*, Khorramabad, 2024.